Bull. Chem. Soc. Jpn., 73, 2243—2253 (2000)

Estimation of Off-Site Coulomb Integrals and Phase Diagrams of Charge Ordered States in the θ-Phase Organic Conductors

Takehiko Mori

Department of Organic and Polymeric Materials, Tokyo Institute of Technology, O-okayama, Tokyo 152-8552

(Received May 10, 2000)

Intermolecular Coulomb repulsion, V, of the highest occupied molecular orbitals (HOMO) of BEDT-TTF (bis(ethylenedithio)tetrathiafulvalene) is calculated for various molecular geometries. The bare V is a quantity that is easily estimated under the point charge approximation. As far as the screened V in actual crystals is proportional to the calculated bare V, the usual θ-phase prefers the horizontal or diagonal stripe, whereas the vertical stripe becomes comparatively stable in the limit of the small dihedral angle (in the metallic limit). The phase diagrams of the θ-phase are discussed under the combination of the static charge distribution (the atomic limit) and the Stoner model (the extended Stoner model). The model contains two order parameters: the spin polarization, S_z, and the charge order, $n-1/2$. This model explains why the insulating state of the Rb salt below 190 K is a paramagnetic charge-ordered state, while the Cs salt has a different insulating phase below 20 K. The lattice dimerization of the Rb salt can be explained only from V.

Recent investigations of the mechanism of metal-insulator (M-I) transitions in organic conductors have refreshed the interest in charge ordered states in these conductors. A charge order has been first suggested in (DIDCNQI)$_2$Ag (DIDCNQI: 2,5-diiodo-*N*,*N*′-dicyanoquinone diimine),[1] and succeedingly in several other one-dimensional organic conductors.[2,3] The particular importance of a charge order has been, however, pointed out in two-dimensional organic conductors such as θ-(BEDT-TTF)$_2$MM′(SCN)$_4$ [BEDT-TTF: bis(ethylenedithio)tetrathiafulvalene; M = Rb, Cs; M′ = Zn and Co].[4,5]

The θ-phase has a donor arrangement in which the molecular planes of the adjacent stacks are tilted alternately in the opposite directions (Fig. 1). A unit cell contains only two donor molecules, and there are only two kinds of intermolecular interactions: the interaction c along the stacking axis, and the interaction p in the diagonal direction. In the θ-phase salts, the M-I transition temperature, T_{MI}, changes as a function of the dihedral angle (θ) between the molecular planes of the adjacent stacks.[6] For example, θ-(BEDT-TTF)$_2$RbM′(SCN)$_4$ [M′ = Zn and Co] with θ = 111° undergoes an M-I transition at 190 K, whereas θ-(BEDT-TTF)$_2$CsM′(SCN)$_4$ with 104° exhibits a transition at 20 K. Since the properties are independent of the second metal atom, M′ (Zn or Co), from now on we shall call the above salts simply the Rb salts and the Cs salts, respectively. Accordingly, all θ-phase salts are located on a single phase diagram (see the bottom of Fig. 12), where the dihedral angle is taken as the horizontal axis. This has been attributed to the change of the bandwidth W, where W increases with a decrease of the dihedral angle.[7] The concept of the universal phase diagram has frequently led to the naive interpretation that the insulator phase is the Mott insulator, and that the M-I transition takes place by changing U/W, (U: on-site Coulomb repulsion).

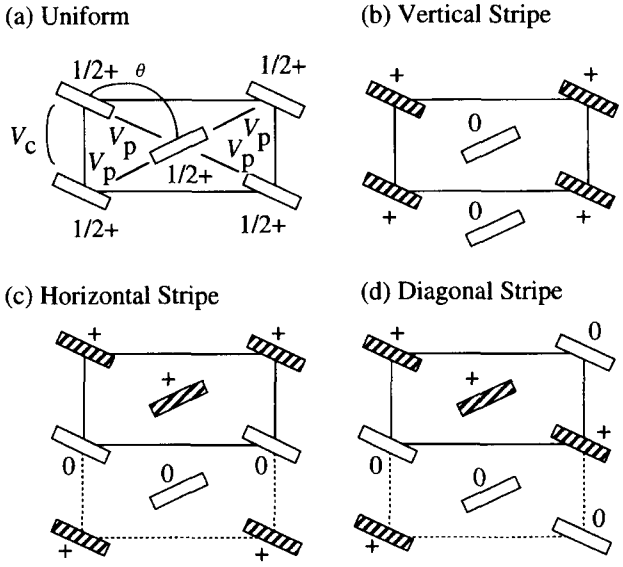

Fig. 1. Stripe patterns of charge ordered states in the θ-phase, viewed along the molecular long axis. (a) Uniform, (b) vertical stripe, (c) horizontal stripe, and (d) diagonal stripe.

Recent experimental results have, however, indicated that the low-temperature insulator phases in these θ-salts are not simple Mott insulators, but charge-ordered states. The NMR spectra show clear splitting, indicating the existence of two kinds of donor molecules with different amount of charges.[8,9] The X-ray diffraction shows that the Rb salts have two-fold periodicity along the stacking axis below T_{MI}.[10] From the comparison of the optical reflectance spectra and the mean-field calculation of the conductivity spectra, Tajima et al. have concluded that the Rb salt has horizontal and vertical charge orders below and above 190 K, respectively, but the

Cs salt belongs to the uniform phase.[11]

Charge order is a phenomenon where disproportionation of charges takes place like $D^{0.5+\delta}D^{0.5-\delta}D^{0.5+\delta}D^{0.5-\delta}$, or in an extreme case like $D^{+}D^{0}D^{+}D^{0}$ as shown in Fig. 1(b)—(d). This is a phenomenon which has sometimes been called charge separation or charge disproportionation. This state is analogous to charge density wave (CDW) states; the CDW state is induced by Fermi surface instability, whereas the charge order is a state primarily produced by the off-site Coulomb interaction, V. The model is based on the extended Hubbard model,

$$H = \sum_i t c_i^{\dagger} c_{i+1} + U \sum_{i\sigma} n_{i\sigma} n_{i\bar{\sigma}} + \sum_i V n_i n_{i+1} \qquad (1)$$

where t represents a transfer integral, U is the on-site Coulomb interaction, and V is the Coulomb repulsion between the site i and $i+1$. $c_i^{\dagger}$, c_i, and n_i are creation, annihilation, and number operators on site i. A charge order may take place, if the third term including V is taken into account. Accordingly, charge-ordered states are essentially paramagnetic. In contrast, the CDW state is usually nonmagnetic, as represented by the Peierls state. Then, a charge ordered state resembles the $4k_F$ CDW state. The CDW state, however, depends on the nesting of the Fermi surface and the dimensionality, whereas the charge order is independent of the dimensionality in principle.

The Fermi surfaces of organic conductors have been discussed on the basis of the simple energy band calculation, where the transfer integrals are estimated from overlap of HOMO, and the band structure is calculated by the tight-binding approximation.[12] Results of this kind of calculation agree well with such experiments as quantum oscillations and angle-dependent magnetoresistance oscillations.[13] In this connection, the author has calculated the overlap integrals of HOMO of two BEDT-TTF molecules by changing the geometry of the BEDT-TTF molecules.[12,14] In the present paper, the intermolecular Coulomb repulsion, V, has been calculated under the same geometrical changes. Particular attention has been paid to the change of V_c and V_p in the θ-phase (Fig. 1(a)), but V in β and $\varkappa$ phases are also estimated.

Phase diagrams of organic conductors have been successfully investigated on the basis of the Hubbard model under the Hartree-Fock approximation.[15—20] Theoretical calculations including V have been carried out along this line,[21] which bring about a variety of charge ordered states. In the present paper, further simplification is attempted by collecting the lowest-order terms of the mean-field theory and by neglecting the details of the band structure. Phase diagrams thus obtained are compared with the calculated V, and the possible charge-ordered states are discussed, particularly in relation to a geometrical change such as the dihedral angle change. The method presented here provides a way to discuss the network of V's explicitly in the real space, without considering the band structure in the reciprocal space.

Method of Calculation

The geometrical parameters of the BEDT-TTF molecules were the same as in our previous reports.[7,14,22] Each molecular orbital calculation was carried out by the extended Hückel approximation. The Slater exponents and the ionization potentials were the same as in our previous reports.[12,14] The one-center and two-center Coulomb integrals between the Slater orbitals were calculated by using an existing routine.[23]

Estimation of V

***V* of Atomic Orbitals.** The off-site Coulomb integral, V, is given by the following two-electron integral:

$$V = \int \phi_1^*(r_1)\phi_1(r_1)\frac{1}{r_{12}}\phi_2^*(r_2)\phi_2(r_2)\mathrm{d}\tau_1\mathrm{d}\tau_2. \qquad (2)$$

In BEDT-TTF conductors, $\phi_i(r)$ is the HOMO of a BEDT-TTF molecule, which is usually represented by a linear combination of atomic orbitals, $\chi_i(r)$:

$$\phi(r) = \sum c_i \chi_i(r). \qquad (3)$$

When Eq. 3 is put in Eq. 2, one- to four-center integrals of the Slater orbitals, $\chi_i(r)$, appear. The three- and four-center integrals are as small as approximately S and S^2 times of the two-center integrals, where S is the overlap integral, and is no more than 0.1 even if the two concerned atoms are directly bonded. From this, all three- and four-center integrals are neglected (complete neglect of differential overlaps), and V is given by,

$$V = \sum_{ij} c_i c_j \int \chi_i^*(r_1)\chi_i(r_1)\frac{1}{r_{12}}\chi_j^*(r_2)\chi_j(r_2)\mathrm{d}\tau_1\mathrm{d}\tau_2. \qquad (4)$$

These one- and two-center integrals are calculated according to the existing routine.[24]

Before discussing the molecular orbital, we shall investigate atomic orbitals. The Coulomb integrals between two sulfur atomic orbitals are calculated as a function of the inter nuclear distance, R (Fig. 2). In the limit of large R, all curves approach the curve of $1/R$. It should be noted that

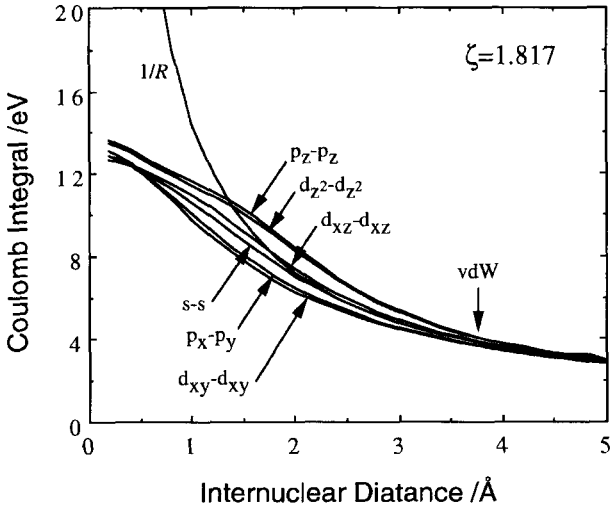

Fig. 2. Two-center Coulomb integrals between two sulfur atomic orbitals, namely 3s, 3p, and 3d Slater orbitals with $\zeta = 1.817$, calculated as a function of inter nuclear distance. The bonding direction is chosen as the z axis.

when R is represented by a.u. (0.529 Å), the Coulomb energy is obtained as $1/R$ in Hartree (27.2 eV). This means that the point charge approximation is appropriate at large distances. Elementary electrostatic theory tells us that, if charge is homogeneously distributed on a sphere, the electrostatic potential generated by the charge is, outside of the sphere, equal to the potential generated by a point charge where all charge is assembled at the center of the sphere. Then the correction to the point charge approximation is in the order of the orbital overlap, which is sufficiently small in the usual intermolecular (van der Waals) distance. In Fig. 2, the deviation from the $1/R$ curve is at most 7% at the van der Waals distance.

In the small R limit, the obtained Coulomb integral deviates from the $1/R$ curve, converging to a finite value at $R = 0$ instead of diverging like $1/R$. This finite value is the on-site Coulomb repulsion, U, of the single atomic orbital. This value is 12.6 eV for the 3s orbital depicted in Fig. 2.

When the atomic orbital is not s, the above electrostatic theory does not apply literally, but Fig. 2 shows that the deviation is small. The s–s curve is closest to the $1/R$ curve. If the orbital is oriented along the bonding axis like p_z–p_z, d_{z^2}–d_{z^2}, and d_{xz}–d_{xz}, where the z axis is chosen as the bonding direction, the curves approach the $1/R$ curve from the upside. When the orbitals spread to different directions like p_x–p_y and d_{xy}–d_{xy}, the curve approaches from the downside.

V of Molecular Orbitals. Figure 3 shows V of two stacked BEDT-TTF HOMO's, calculated as a function of the interplanar distance, ΔZ. The points designated by V ($D = 1.6$ Å) are calculations according to Eq. 4, where all two-center integrals are estimated. In order to simulate the actual stack, the molecules are slid by $D = 1.6$ Å along the molecular long axis. These points are very close to the curve designated as "$1/R$ point charge approximation," within 2% error, where all two-center integrals between the atomic orbitals are approximated by $1/R$, and Eq. 4 is approximated as

$$V = \sum c_i c_j \frac{1}{R_{ij}}. \tag{5}$$

Here the charges on the HOMO are distributed on the centers of each atom. If we assemble all charges on the center of the molecule, the distance between the molecular centers, R_0, gives the Coulomb repulsion, which is depicted in Fig. 3 as the $1/R_0$ curve. Figure 3 shows that even this approximation is not far from the results of Eqs. 5 and 4. It is also a merit of this approximation that the results are independent of c_i, namely the molecular orbital calculation. Even if one does not have any computer program, one can obtain a good estimate of V from the inverse of the intermolecular distance, R_0. It is also noteworthy that V is a long range function of R owing to the $1/R$ dependence; V has a considerable magnitude even above $R > 20$ Å. On the contrary, the overlap integral, S, follows $e^{-\zeta R}$, rapidly falling to zero even below 5 Å (Fig. 3).

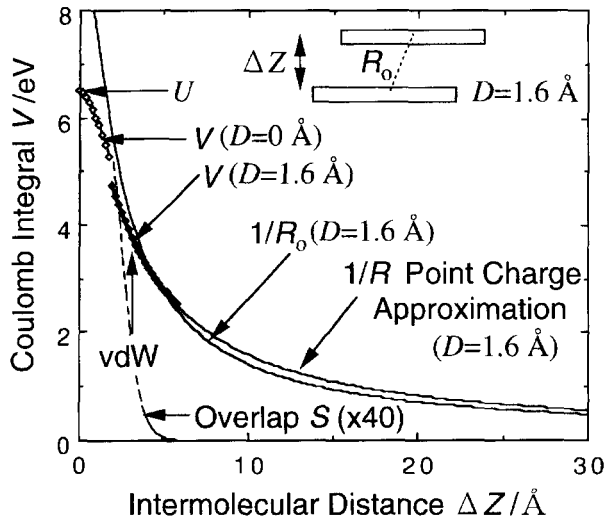

Fig. 3. Intermolecular Coulomb integral, V, between HOMO of two stacked BEDT-TTF molecules, calculated as a function of the intermolecular distance, ΔZ. Points designated by V represent the straightforward integration according to Eq. 4, $1/R$ is the point charge approximation for each atom (Eq. 5), and $1/R_0$ is the point charge approximation for molecules, where all charges are assembled to the molecular centers. All calculations are carried out for $D = 1.6$ Å (D: the displacement along the molecular long axis, see the inset), except for the V ($D = 0$ Å) points, which then gives U in the limit of $\Delta Z = 0$ Å.

In the small ΔZ limit, the $1/R_0$ curve diverges to infinity, but the V curve goes to a finite value, $U = 6.49$ eV at $\Delta Z = 0$ Å. In order to estimate U, we cannot use Eq. 5, because Eq. 4 contains one-center integrals ($i = j$). In this connection, U is a quantity that largely depends on the used basis functions. Castet et al. have reported that U of BEDT-TTF is 4.64 eV,[24] whereas the same quantity is 5.9 eV in Ref. 25. By contrast, V is estimated only from two-center integrals, and can be approximated by Eq. 5. As a consequence, V does not much depend on the basis functions. In the following calculations, V will be estimated by using Eq. 5.

It should be noted that the values obtained here are bare values without the screening by conduction electrons. The experimental V is expected to be about one quarter of the experimental U; the latter is believed to be 0.8 to 1.0 eV from various experiments. Consequently, the experimentally expected V is in the order of 0.1 to 0.3 eV,[11] which is less than one-tenth of the bare values. Since the calculation of U is not very reliable, we could not estimate V/U from the calculation. If the screened V is proportional to the calculated bare V, however, we can straightforwardly compare the calculated V with the phase diagrams presented in the later sections. At least we can assume that the qualitative tendency of the geometrical dependence of V as well as the charge orders in the extreme limits will be unchanged even for the screened V.

Geometrical Dependence of V. In Refs. 7 and 14, we have calculated the intermolecular overlap integrals by changing the geometry of two BEDT-TTF molecules. Here, V is calculated under the same geometrical change.

Figure 4 shows V between two parallel BEDT-TTF molecules, where one BEDT-TTF molecule is rotated around the long axis of another BEDT-TTF molecule. The angle,

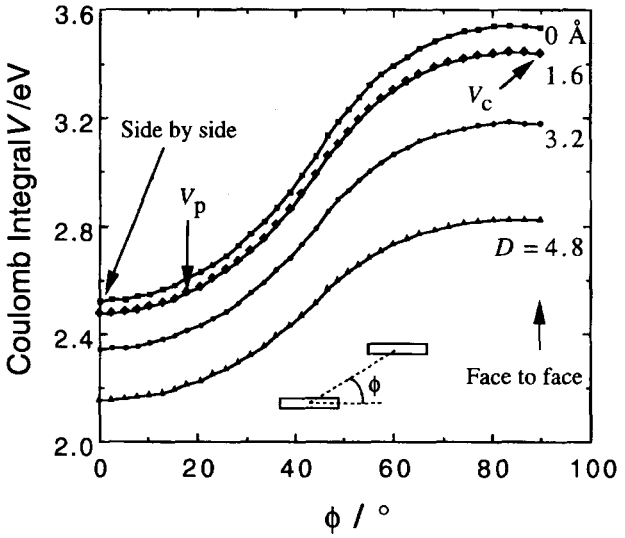

Fig. 4. Intermolecular Coulomb integral, V, between HOMO of two parallel BEDT-TTF molecules, calculated as a function of the angle between the molecular plane and the intermolecular vector, ϕ (see the inset, viewed along the molecular long axis).

ϕ, between the molecular plane and the direction to another BEDT-TTF, is changed from the side-by-side arrangement $\phi = 0°$ to the face-to-face stacking, $\phi = 90°$. The geometrical change is the same as Fig. 2(a) in Ref. 14. The overlap integral changes sign three times around 15°, 40°, and 70° on account of π-character of the HOMO.[14] On the contrary, V in Fig. 4 monotonously increases with the increase of ϕ. This is reasonable because the distance between the molecular centers, R_0, decreases from 6.6 Å at the side-by-side arrangement to 3.6 Å at the face-to-face arrangement. As a consequence, V in β and β''-phases is expected to be largest along the stacking axis, and smallest in the transverse direction.

The dihedral angle dependencies of V and t in θ-phases are shown in Fig. 5. The lattice constants are changed with θ according to Eq. 2 in Ref. 7. Then the curve of t_p in Fig. 5(b) is the same as the previous calculation (Fig. 3 in Ref. 7). The transfer integral, t, is estimated from $t = ES$, where S is the overlap integral, and $E = -10$ eV is the energy of HOMO. In Fig. 5, t_c is also plotted. At $\theta = 180°$, t_c is overwhelmingly large, because this corresponds to a face-to-face arrangement. t_c changes sign twice around $\theta = 135°$ and 105°, but in the θ range of the actual θ-phase ($130° > \theta > 98°$), the absolute value of t_c is not much larger than t_p. As shown in Ref. 7, the bandwidth, W, is $8|t_p|$ as far as $t_c < |t_p|$, so that t_p is much more important than t_c in determining W.

Under the same geometrical change, V is calculated (Fig. 5(a)). The value of V_c at $\theta = 180°$ is large; this corresponds to the face-to-face stack ($\phi = 90°$ and $D = 0$ Å in Fig. 4). As θ decreases, V_c decreases, and V_p increases. In the actual θ range of the θ-phase, V_c is still larger than V_p, but near the metallic limit ($\theta = 90°$) the V_c curve crosses the V_p curve. The crossing point may, however, move owing to the anisotropic screening. As shown in Fig. 5, the p interaction is predominant as a transfer, but V_c is more important as the Coulomb repulsion. These results will be discussed later in comparison with the phase diagrams.

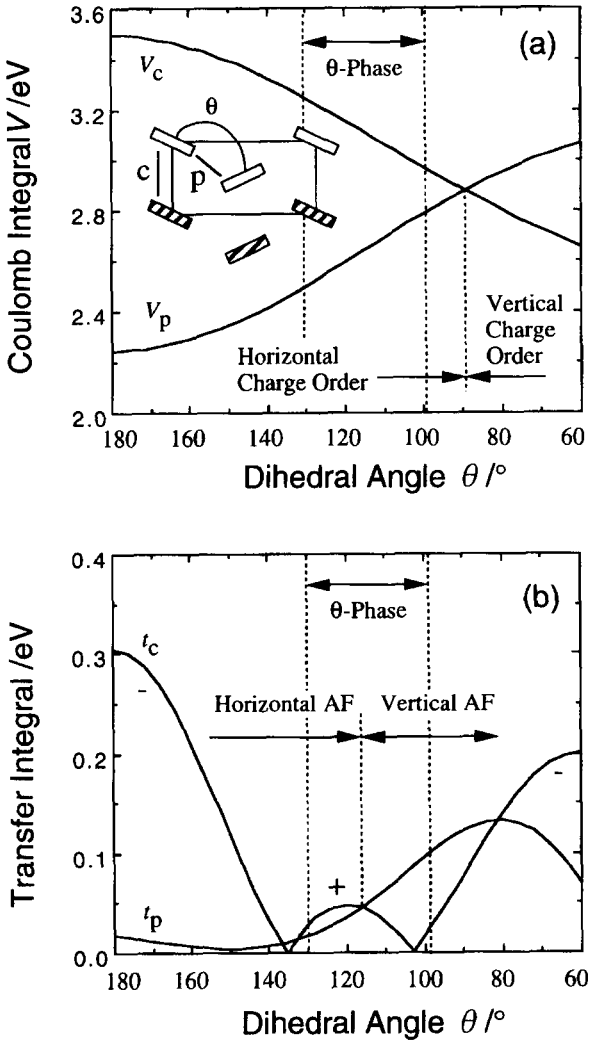

Fig. 5. (a) Intermolecular Coulomb integrals, V, and (b) transfer integrals, t, between HOMO of two tilted BEDT-TTF molecules, calculated as a function of the dihedral angle, θ, in the θ-phase. The intermolecular distances are changed according to Eq. 2 of Ref. 7.

In order to discuss overlap integrals in $\varkappa$-phase, we have calculated the overlap integrals between two vertical BEDT-TTF molecules (Fig. 10 in Ref. 7). Figure 6 is the same calculation for V, where a vertical BEDT-TTF is slid along Y' (see the inset of Fig. 6). When Y' is 0 Å, V is largest, where the distance between the molecular centers, R_0, is 5.0 Å. As Y' increases, V monotonically decreases. These results are convincing in view of the change of R_0.

The results in Figs. 4, 5, and 6 indicate that V is a classical quantity; it is always positive and a smooth function of the geometry. This contrasts with t, which changes sign frequently depending on the sign of the orbitals. This is a quantum mechanical quantity in a sense. Consequently, V is expected to be not much dependent on the parameters used in the molecular orbital calculation.

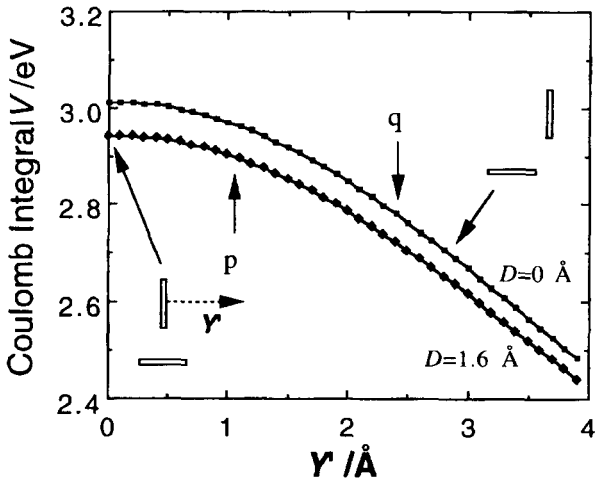

Fig. 6. Intermolecular Coulomb integral, V, between HOMO of two perpendicular BEDT-TTF molecules, calculated as a function of Y' (see the inset, viewed along the molecular long axis).

Phase Diagrams

Phase Diagram in the Atomic Limit. The extended Hubbard model represented by Eq. 1 affords various ground states. Although exact solution of this model is clearly beyond the level of the present paper, we shall discuss the qualitative features. In the following, we shall start from the simplest case, and proceed to more complicated cases.

In the first place, we shall investigate the static or atomic limit of Eq. 1, where the first kinetic energy term (namely t) is neglected in comparison with the second and the third terms (namely V and U). In the Hartree-Fock theory, the electron numbers are approximated as

$$n_i n_j = n_i\langle n_j\rangle + \langle n_i\rangle n_j - \langle n_i\rangle\langle n_j\rangle. \tag{6}$$

Then Eq. 1 is diagonalized, and can be solved after iteration, which determines n_i self consistently. Here, however, we shall only pay attention to the lowest order term of the Hartree-Fock approximation, and we shall further approximate Eq. 6 to

$$n_i n_j = \langle n_i\rangle\langle n_j\rangle. \tag{7}$$

The meaning of this approximation will be discussed in the later.

In the second place, we shall consider the spin non polarized case. The number operators in the U term (Eq. 1) are restricted to up or down spins, but the numbers of up (or down) spin electrons are assumed to be half of the total electrons.

$$\langle n_{i\uparrow}\rangle = \langle n_{i\downarrow}\rangle = \frac{1}{2}\langle n_i\rangle. \tag{8}$$

With these approximations, the potential energy terms of Eq. 1 are represented by

$$E = \frac{1}{4}U\sum\langle n_i\rangle\langle n_i\rangle + \sum V\langle n_i\rangle\langle n_j\rangle. \tag{9}$$

In the third place, we shall start from the complete charge separation, where, as shown in Fig. 1, the charges are separated to D^0 and D^+. This restriction is, however, easily removed in the later section. The names of the stripe patterns, according to Seo, are shown in Fig. 1.[21]

As shown in Fig. 1, $\langle n_i\rangle$ is 0, 1/2, or 1. The potential energy, E of the uniform state per unit cell is

$$\text{Uniform}: \quad E = 2\times\frac{1}{4}U\times\frac{1}{2}\times\frac{1}{2}+4V_p\frac{1}{2}\times\frac{1}{2}+2V_c\frac{1}{2}\times\frac{1}{2}$$
$$= \frac{U}{8}+V_p+\frac{V_c}{2}, \tag{10}$$

where the factor 2 before U is the number of molecules in a unit cell, and 4 and 2 before V_p and V_c are the number of interactions in a unit cell. The factor, 1/4, in the U term comes from the spin non polarization (Eqs. 8 and 9). Similarly, for the vertical stripe,

$$\text{Vertical}: \quad E = \frac{1}{4}U(1\times1+0\times0)+4V_p(1\times0)+V_c(1\times1+0\times0)$$
$$= \frac{U}{4}+V_c. \tag{11}$$

The energies for the diagonal and horizontal stripes have to be calculated for the doubled cell, but the value per one unit cell is

$$\text{Diagonal} = \text{Horizontal}:$$
$$E = \frac{1}{2}\left[\frac{1}{4}U(2\times1\times1+2\times0\times0)+V_p(2\times1\times1+4\times1\times0+2\times0\times0)\right.$$
$$\left.+V_c(4\times1\times0)\right]$$
$$= \frac{U}{4}+V_p. \tag{12}$$

The energy is the same for the diagonal and horizontal stripes, so that we cannot distinguish these states within our approximation.

Among Eqs. 10—12, the states with the lowest energy are realized. The conditions are

$$\text{Uniform} < \text{Vertical}:$$
$$\frac{U}{8}+V_p+\frac{V_c}{2} < \frac{U}{4}+V_c \rightarrow 8V_p-4V_c < U, \tag{13a}$$
$$\text{Uniform} < \text{Diagonal}: \quad 4V_c < U, \tag{13b}$$
$$\text{Vertical} < \text{Diagonal}: \quad V_c < V_p. \tag{13c}$$

From this, the phase boundaries are obtained as shown in Fig. 7. When U is sufficiently large, the uniform state is stable. This is reasonable, because the charge-ordered states increase the U term. The boundaries are given by $U = 8V_p - 4V_c$ or $U = 4V_c$.

If V is comparatively large, the charge ordered states appear. When V_p is larger than V_c, the vertical stripe is stable. The vertical stripe eliminates the V_p term, because charge on every other chain is zero. On the other hand, the vertical stripe enhances the V_c term, but this is unimportant because $V_p > V_c$. On the contrary, the condition, $V_p < V_c$, leads to the diagonal or horizontal stripe. From this, we can extract a simple and general rule: *When charge ordering takes place, the charge orders in the direction of the smallest V.*

As shown in Fig. 5, in the region of the actual θ-phase, V_c is larger than V_p. Then the horizontal (or diagonal) charge

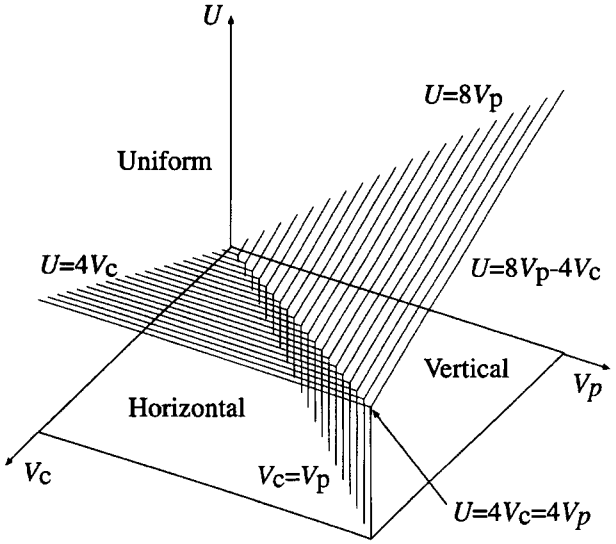

Fig. 7. Phase diagram of charge ordered states in the θ-phase. For the extended Stoner model, the vertical axis, U, is modified to the smaller of U or W.

order is expected. The curves of V_c and V_p cross around $\theta = 90°$, below which the vertical charge order is possible (Fig. 5). If the screening is anisotropic, the ratios of the screened V's may be different from the ratios of the calculated V's. In this connection, on account of the difference between t_p and t_c, the phase boundaries of the horizontal and vertical phases obtained from the Hartree-Fock calculations slightly shift from the present result, $V_p = V_c$.[11,21] Since the crossing point of the V_c and V_p curves moves to the left owing to the anisotropic transfer integrals ($t_p > t_c$), the vertical charge order may appear near the metallic limit of the actual θ-phase.

Tajima et al. have concluded from reflectance spectra that the insulating phase of the Rb salt below 190 K has the horizontal charge order.[11] This agrees with the above phase diagram. They have also suggested that the metal phase of the Rb salt above 190 K has the vertical charge order. Owing to the thermal contraction, upon cooling, the dihedral angle increases, and a particularly large increase is observed at the 190 K transition. Then the system moves from the right to the left in Fig. 5(a). Qualitatively this is in agreement with the change from the vertical to the horizontal charge orders predicted by the present calculations.

Atomic Limit in the β''-Phase. It is instructive to investigate the charge order in the β''-phase. The actual β''-phases in BEDT-TTF conductors are dimerized to some extent, but we consider a uniform β''-phase (Fig. 8). Such β''-phases (β''_{10}-phase in the notation of Ref. 14) have been known in some BO (bis(ethylenedioxy)tetrathiafulvalene) salts.[14] The β''-phase has intermolecular interactions in three different directions: p, q and c in Fig. 8. The potential energies of stripes in Fig. 8 are

$$\text{Uniform}: \quad E = \frac{1}{2}\left[\frac{U}{4} + V_p + V_c + V_q\right], \tag{14a}$$

$$\text{Vertical}: \quad E = \frac{U}{4} + V_p, \tag{14b}$$

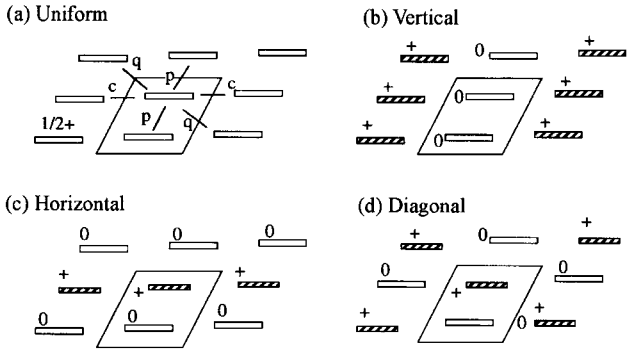

Fig. 8. Stripe patterns of charge ordered states in the β''-phase, viewed along the molecular long axis. (a) Uniform, (b) vertical stripe, (c) horizontal stripe, and (d) diagonal stripe.

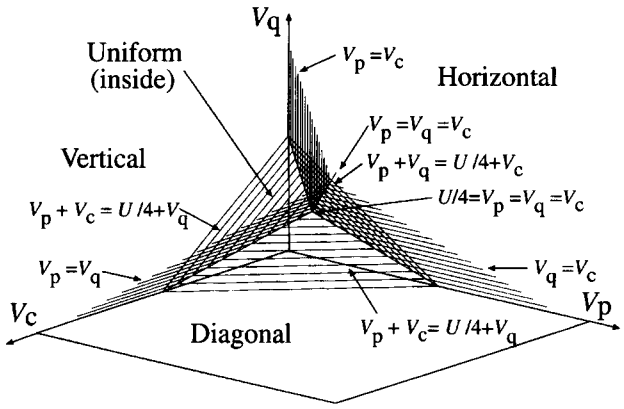

Fig. 9. Phase diagram of charge ordered states in the β''-phase. The uniform state is stable in the region near the origin, surrounded by $V_c+V_q < U/4+V_p$, $V_c+V_p < U/4+V_q$, and $V_p+V_q < U/4+V_c$. Out of this region, the smallest V determines the direction of the charge order.

$$\text{Horizontal}: \quad E = \frac{U}{4} + V_c, \tag{14c}$$

$$\text{Diagonal}: \quad E = \frac{U}{4} + V_q. \tag{14d}$$

The smallest among Eqs. 14b to 14d is that having the smallest V. Consequently, if a charge order takes place, the charge orders in the direction of the smallest V. This is the generalization of the above-mentioned rule.

The boundary between the charge-ordered state and the uniform state is obtained as follows. For instance, we assume that the smallest V is V_p. Then comparing Eq. 14b with Eq. 14a, the phase boundary is obtained as

$$\text{Uniform} < \text{Vertical}: \quad V_c + V_q < \frac{U}{4} + V_p. \tag{15}$$

Here the smallest V appears in the right side, and is added to $U/4$, while other V's come to the left side. If U is sufficiently large, this gives rise to the uniform state. The phase diagram is depicted in Fig. 9, which is plotted with respect to three V's. The region surrounded by $V_c+V_q = U/4+V_p$, $V_p+V_q = U/4+V_c$, and $V_p+V_c = U/4+V_q$, is the uniform state. In this region, V's are so small (close to the origin) that the uniform state is stable. It should be noted that we consider

only positive U and V's. Out of this region, charge orders occur, and the direction of the charge order is the direction of the smallest V.

When we put $V_p = V_q$ in Eq. 15, this gives $4V_c < U$. This equals Eq. 13b for the θ-phase. This means that the θ-phase is a special case of the β''-phase where two of the three directions are put equivalent. This is obvious by comparing Figs. 1 and 8. For calculating the potential energy, the directions of the molecular planes are unimportant, and E is obtained only from the network of V's. Then Fig. 7 is regarded as a special case of Fig. 9. This is the reason that, in Fig. 7, the boundary between the uniform and the vertical stripe is given by $U = 8V_p - 4V_c$; $8V_p$ is the sum for the two directions ($2\times4V_p$), and $-4V_c$ come from the right side of Eq. 15.

Fractional Charge. In the actual system, the charge order is not complete like $D^+D^0D^+D^0$, but is fractional like $D^{0.5+\delta}D^{0.5-\delta}D^{0.5+\delta}D^{0.5-\delta}$. We shall take this into account; as shown in Fig. 10(a), the charges are put as n_1 and n_2. From the charge conservation, $n_1+n_2 = 1$; n_1 is put as n, and the number of variables is reduced to one. The potential energy of the vertical stripe (Fig. 10(a)) is then,

$$\text{Vertical}: \quad E = \frac{1}{4}U(n_1^2+n_2^2) + 4V_p n_1 \times n_2 + V_c(n_1^2+n_2^2)$$
$$= \left(\frac{U}{2}+2V_c-4V_p\right)\left(n-\frac{1}{2}\right)^2 + \frac{U}{8}+V_p+\frac{V_c}{2}. \quad (16)$$

When $n = 1/2$, this equation correctly gives the energy of the uniform state (Eq. 10). When n is put 0 or 1, this equation reduces to Eq. 11. Equation 16 is quadratic with respect to $n-1/2$, so that the energy minimum depends on the sign of the coefficient of the $(n-1/2)^2$ term. If $U/2+2V_c-4V_p$ is positive, obviously $n = 1/2$ is the energy minimum. When $U/2+2V_c-4V_p$ becomes negative, n deviates from 1/2, resulting in charge separation. The boundary $U/2+2V_c-4V_p = 0$ is the same as Eq. 13a. The energy of the horizontal or diagonal charge order is similarly obtained (Fig. 10(b)).

$$\text{Horizontal} = \text{Diagonal}: \quad E = \left(\frac{U}{2}-2V_c\right)\left(n-\frac{1}{2}\right)^2 + \frac{U}{8}+V_p+\frac{V_c}{2}. \quad (17)$$

The sign of the first term gives the same boundary as Eq. 13b. Therefore, the phase diagrams which we have obtained for complete charge separation are valid even for the fractional charge separation.

In Eqs. 16 and 17, once the charge order takes place, the charge separates as much as possible to a degree that is limited by other unconsidered factors. This happens because we have assumed Eq. 7. If we assume Eq. 6, or perterbatively estimate the higher order terms, the potential energy is expressed as

$$E = A\left(n-\frac{1}{2}\right)^2 + B\left(n-\frac{1}{2}\right)^4 + . \quad (18)$$

This is the Ginzburg–Laudau expansion of the potential energy with respect to the order parameter, $n-1/2$. When $A > 0$, $n = 1/2$ gives the energy minimum. When $A < 0$, $n-1/2$ becomes non-zero. In this case, n does not necessarily jump to the maximum and minimum values. As long as B is non-zero, $n-1/2$ which gives the energy minimum grows in proportion to $\sqrt{|A|/B}$. Then a second order phase transition takes place. If a $(n-1/2)^3$ term is added, a first order transition occurs. What we have done in the above discussion is the estimation of A, the sign of which gives the correct phase boundary.

Spin Polarization. So far we have not considered spin polarization, namely we have assumed Eq. 8. Here we consider that the numbers of electrons with upward and downward spins are different.

$$n_{1\uparrow}+n_{1\downarrow} = n_1, \quad n_{2\uparrow}+n_{2\downarrow} = n_2 \quad (19)$$

The degree of spin polarization is expressed by S_z,

$$n_{1\uparrow} = n_1\left(\frac{1}{2}+S_z\right), \quad n_{1\downarrow} = n_1\left(\frac{1}{2}-S_z\right)$$
$$n_{2\uparrow} = n_2\left(\frac{1}{2}-S_z\right), \quad n_{2\downarrow} = n_2\left(\frac{1}{2}+S_z\right) \quad (20)$$

The following theory (Eq. 21) does not depend on the orientation of spins, namely the signs of S_z in the above equation. The magnetic structure will be independently determined in the later section from J's. The potential energy at the atomic limit is obtained similarly to the preceding section. For instance, in the vertical stripe (Fig. 10(c)),

$$\text{Vertical}: \quad E = \frac{1}{4}U\left(n_1^2\left(\frac{1}{2}+S_z\right)\left(\frac{1}{2}-S_z\right)+n_2^2\left(\frac{1}{2}-S_z\right)\left(\frac{1}{2}+S_z\right)\right)$$
$$+4V_p\, n_1 \times n_2 + V_c(n_1^2+n_2^2)$$
$$= \left(2U\left(\frac{1}{4}-S_z^2\right)+2V_c-4V_p\right)\left(n-\frac{1}{2}\right)^2$$
$$+\frac{U}{8}+V_p+\frac{V_c}{2}. \quad (21)$$

where we have used $n_1+n_2 = 1$, and n_1 is put as n. The only difference between this equation and Eq. 16 is that $4(1/4-S_z^2)$

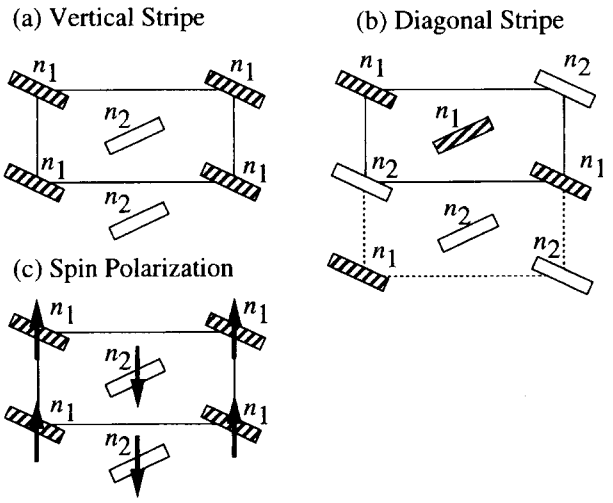

Fig. 10. Stripe patterns of charge ordered states with fractional charges in the θ-phase: (a) vertical and (b) diagonal stripes. (c) Spin polarization coexisting with vertical charge order.

is multiplied with the U term.[26] If there is no spin polarization ($S_z = 0$), Eq. 16 is recovered. If complete spin polarization takes place ($|S_z| = 1/2$), the U term becomes zero. This is reasonable because no double occupancy occurs under the complete spin polarization. If U is put zero in Fig. 7, charge ordered states are always stable. In the actual system, however, the spin polarization competes with the kinetic energy. This will be taken into account in the next section.

It is characteristic of the quarter-filled band that the spin polarization, S_z, and the charge order, $n-1/2$, are entirely independent. In a half-filled band, S_z is restricted by the charge order. For example, under the complete charge separation like D^0D^{2+}, S_z must be zero. This is the reason that such simple treatment as Eq. 21 is possible in the quarter-filled band.

Stoner Model. We shall treat the Hubbard model, which contains the t and U terms but not the V term in Eq. 1, within the mean-field approximation. We assume that the energy band is not affected by U; then, as shown in Fig. 11, the energy bands of up and down spin electrons shift mutually by 2Δ. This model has been known as the Stoner model.[27] According to the usual notation of the Stoner model, the magnetization, m, is,

$$m = n_\uparrow - n_\downarrow = \int_{E_F-\Delta}^{E_F+\Delta} D(E)\mathrm{d}E = 2D\Delta \tag{22}$$

where $D = D(E_F)$ is the density of states at the Fermi level, E_F. The magnetization, m, is connected to S_z like $S_z n = m/2$, as obtained from Eqs. 20 and 22. The loss of the kinetic energy induced by the band shift like Fig. 11 is,

$$\begin{aligned}\Delta E &= \int_0^{E_F+\Delta} ED(E)\mathrm{d}E + \int_0^{E_F-\Delta} ED(E)\mathrm{d}E - 2\int_0^{E_F} ED(E)\mathrm{d}E \\ &= \int_{E_F-\Delta}^{E_F+\Delta} ED(E)\mathrm{d}E = D\Delta^2 = \frac{m^2}{4D} = \frac{Wm^2}{4},\end{aligned} \tag{23}$$

where Eq. 22 is used, and $W = 1/D$ is assumed to be the band width. This applies exactly when the density of states is constant with respect to E, like the two-dimensional free-electron model (Fig. 11), but the following theory works generally if we use $1/D$ instead of W. The U term is easily obtained from the definition of m (Eq. 22) and $n = n_\uparrow + n_\downarrow$,

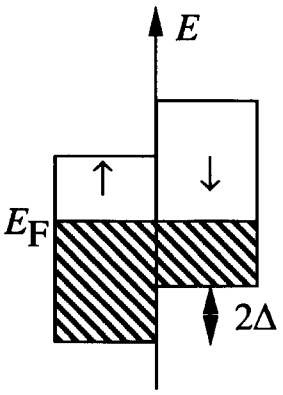

Fig. 11. Energy difference 2Δ of the up and down spin energy bands in the Stoner model.

$$E = Un_\uparrow n_\downarrow = \left(\frac{U}{4}\right)(n^2 - m^2). \tag{24}$$

Summation of Eqs. 23 and 24 gives the total energy.

$$\Delta E = \frac{Wm^2}{4} + \frac{U}{4}(n^2 - m^2) = \left[\frac{W-U}{4}\right]m^2 + \frac{U}{4}n^2 \tag{25}$$

The second term is constant as long as the total electron number, n, is unchanged. The first term is quadratic with respect to m, affording the A term in the Ginzburg–Landau expansion (Eq. 18). When $W > U$, the coefficient of the m^2 term is positive, resulting in no spin polarization ($m = 0$). When $W < U$, the m^2 term is negative, giving rise to spin polarization.

Strictly speaking, the Stoner model predicts a transition from a paramagnetic metal to a ferromagnetic metal. An antiferromagnetic state becomes stable above a limit U_{AF} which is different from the Stoner condition, $U_F = 1/D = W$. In the quarter-filling, when the Hartree–Fock approximation is adopted, U_F is usually smaller than U_{AF}, namely the ferromagnetic state is more stable than the antiferromagnetic state.[28,29] Then we shall take U_F to be the condition of the spin polarization.

Mean-Field Phase Diagram. Following the above discussion, we can take the kinetic energy into account, by adding $Wm^2/4 = W(S_z n)^2$ to the U term. Then Eq. 21 becomes

$$\begin{aligned}E = 2&\left[(W-U)S_z^2 + \frac{U}{4} + V_c - 2V_p\right]\left(n - \frac{1}{2}\right)^2 \\ &+ \frac{1}{2}(W-U)S_z^2 + \frac{U}{8} + V_p + \frac{V_c}{2}.\end{aligned} \tag{26}$$

for the vertical stripe. $V_c - 2V_p$ is replaced by $-2V_c$, when V_c is larger than V_p, and the horizontal or diagonal stripe is more stable than the vertical stripe. This model can be derived if we assume that the energy band is not affected by U and V. This may thus be called the extended Stoner model.

This equation is quadratic with respect to both S_z and $n-1/2$, and the condition of the spin polarization is the same as for the Stoner model. When $W > U$, S_z is zero, and Eq. 26 reduces to Eq. 16. When $W < U$, the most stable state appears at $|S_z| = 1/2$, and the coefficient of the first term of Eq. 26 becomes $W/2 + 2V_c - 4V_p$. This is the same as the coefficient of Eq. 16, if U is replaced by W. These considerations modify Fig. 7 only at one point; the vertical axis is not simply U, but is replaced by the smaller of U and W. With this modification, the phase diagram of Fig. 7 is valid.

Several ground states derived from Eq. 26 are shown in Fig. 12. This phase diagram is depicted for U, W, and the smaller of $4V_c$ and $8V_p - 4V_c$. Spin polarization (SP) occurs when $U > W$. In this left upper region, the charge order (CO) takes place if $4V_c$ (or $8V_p - 4V_c$) is larger than W. It should be noted that the smaller of U and W is compared with $4V_c$. On the contrary, $U < W$ leads to non spin polarized states (NSP), in which $4V_c > U$ gives rise to the charge order. Then four different states appear; U+NSP is a simple metal state, U+SP corresponds to a spin polarized state without a charge order, CO+SP is a paramagnetic charge ordered state, which is, in a sense, an analog of $4k_F$ charge-density

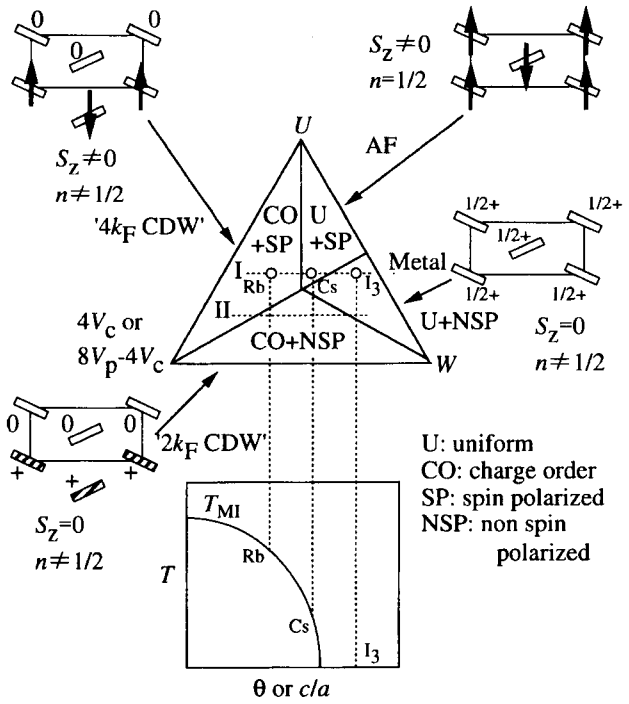

Fig. 12. Phase diagram of the θ-phase under the extended Stoner model, together with the universal phase diagram. The latter is derived from the line I (or II) of the former phase diagram.

wave (CDW) state in a one-dimensional system, and finally CO+NSP is a non magnetic charge-ordered state analogous to $2k_F$ CDW state in one dimension. The last has been called a "bipolaronic insulator" by Seo.[23] The charge ordered phases are essentially regarded as insulating, but the U+SP state should be a ferromagnetic metal in the original Stoner model. At this position, however, we expect some kind of spin polarized state, such as an antiferromagnetic metal or an antiferromagnetic insulator. The charge order occurs only when V is finite; along the edge between U and W in Fig. 12, the charge order does not occur except for the U infinite limit.[30]

In the actual θ-phase salts, the insulating state of the Rb salt below 190 K has been attributed to the horizontal stripe from both optical and NMR measurements.[9,11,31] This corresponds to the CO+SP state in Fig. 12. For the Cs salt, there is some discussion about the origin of the insulating state below 20 K. A Mott insulating state has been suggested from NMR study;[32] this seems in agreement with the absence of a charge order indicated by the optical measurements.[11] If we follow this interpretation, the 20 K state of the Cs salt corresponds to the U+SP phase in Fig. 12. The metallic salts such as θ-(BEDT-TTF)$_2$I$_3$ are located in the U+NSP region. Therefore, line I in Fig. 12 affords the universal phase diagram of the θ-phase depicted at the bottom of Fig. 12. This explains why the Rb salt and the Cs salt have different insulating states in the universal phase diagram.

It is not obvious from experiments that the lines I and II are horizontal in Fig. 12. U is, however, expected to be constant for a given donor. As shown in Fig. 5, on going from the left to the right, V_c decreases, and the bandwidth (t_p) increases. Then the universal phase diagram is regarded as a consequence of the competition between V and W, although U remains essentially constant. This is the reason that the lines I and II are approximately horizontal in Fig. 12.

Nakamura et al. have recently suggested, on the basis of ESR and NMR investigations, that the 20 K state of the Cs salt is a non-magnetic charge ordered state.[33] This corresponds to CO+NSP in Fig. 12. When cooled to 20 K, the Rb salt also undergoes another transition to a nonmagnetic state (CO+NSP), which has been called the spin-Peierls state.[6,34] This suggests the possibility that, upon cooling, the line I drops to the line II in Fig. 12. In this interpretation, the ground states below 20 K are the same for both Rb and Cs salts. Further experimental works are desired to determine the ground state of the Cs salt unambiguously.

It is noteworthy that the horizontal charge order depicted in Fig. 12 has a doubled cell along the vertical axis. This lattice dimerization is caused only by V. The role of lattice distortion has been emphasized in Ref. 20, but it is, at least in principle, possible that V is the only origin of the dimerization. In the case of $V_p > V_c$, however, the charge order which is not accompanied by the lattice dimerization takes place.

Figure 12 does not contain any information about the molecular network except for the form of the V term. If one-dimensional fluctuations are not taken into account, this phase diagram is valid even in one dimension, where the V term is replaced by $2V$. This is the reason that the line I in Fig. 12 shows qualitative agreement with Jerome's phase diagram of (TMTTF)$_2$X and (TMTSF)$_2$X salts, where U+SP is regarded as the SDW state, and CO+SP is understood as the charge localized state (TMTTF: tetramethyltetrathiafulvalene; TMTSF: tetramethyltetraselenafulvalene).[35] The dimerization, however, complicates the physics; in particular superconductivity mediated by spin fluctuation does not appear without dimerization.[36]

It should be emphasized that the above simple treatment is possible only in the uniform quarter-filled system, in which the spin polarization and the charge order behave independently. In the half-filled case, the spin polarization and the charge order are competitive. As a consequence, the CO+SP phase will shrink on account of the other phases. Dimerization leads to an effectively half-filled band, as expected in the $\varkappa$-phase,[37] giving rise to the same influence. The investigations under the mean-field approximation have demonstrated that the dimerization stabilizes the antiferromagnetic state.[15–21] In the present paper, lattice distortion and electron-phonon interactions are not explicitly considered. This does not, however, mean that these effects are unimportant.

Magnetic Structure. We shall discuss possible magnetic structures of the θ-phase. The total energy given by, say, Eq. 21 does not depend on orientation of spins.[28] We have discussed the spin polarization, but in the static limit, ferromagnetic and antiferromagnetic arrangements afford the same energy. The stable magnetic structure should be determined from magnetic interaction J, which is given from the transfer integrals as $J = -2t^2/U$. Since t has been obtained in

Fig. 5(b), we can expect the possible magnetic structures, if the phase diagram of the stable magnetic structure is known in relation to J's.

The magnetic phase diagram is easily obtained from the conventional mean field theory. Although there is a more elegant way, we will investigate the relative stability of various magnetic structures in the same way as we have done for the charge ordered states. The spin Hamiltonian is

$$H = -2\Sigma J_{ij} S_i S_j. \tag{27}$$

When we put the ferromagnetic spin alignment in Eq. 27, the energy per unit cell is,

Ferromagnetic :

$$E = -2\left[2J_c\left(\frac{1}{2}\right)\left(\frac{1}{2}\right)+4J_p\left(\frac{1}{2}\right)\left(\frac{1}{2}\right)\right] = -J_c - 2J_p. \tag{28}$$

Similarly, the energies of other magnetic structures are:

$$\text{Horizontal :} \qquad E = J_c \tag{29}$$

$$\text{Vertical :} \qquad E = -J_c + 2J_p. \tag{30}$$

Among Eqs. 28—30, the state with the lowest energy is realized. This affords the phase boundaries as:

$$\text{Ferromagnetic} < \text{Vertical :} \quad -J_c - 2J_p < -J_c + 2J_p \rightarrow J_p > 0 \tag{31a}$$

$$\text{Ferromagnetic} < \text{Horizontal :} \quad J_p > -J_c \tag{31b}$$

$$\text{Horizontal} < \text{Vertical :} \quad J_p > J_c. \tag{31c}$$

This determines the phase diagram in Fig. 13. When both J_c and J_p are positive, the ferromagnetic phase is stable. If only J_p becomes negative, the vertical antiferromagnetic (AF) structure becomes stable. The boundary between the vertical and the horizontal AF is given by $J_p = J_c$. If a tilted magnetic cell is taken, the diagonal alignment appears instead of the horizontal alignment, but these spin structures have the same energy, and cannot be distinguished within the present approximation.

The calculations of the transfer integrals in Fig. 5(b) indicate that in the small θ region ($\theta < 117°$, namely near the metallic limit), $t_p > t_c$ and $|J_p| > |J_c|$ with negative J_p and J_c, leads to the vertical AF phase. Contrarily the insulating limit ($\theta > 117°$) prefers the horizontal (or diagonal) AF

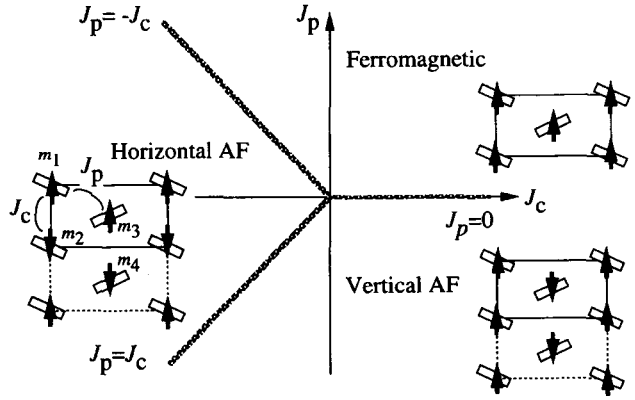

Fig. 13. Mean-field magnetic phase diagram of the θ-phase.

phase. In the actual θ-phase, no phase is clearly identified to an AF phase, but the above discussion provides the possible magnetic structures in the θ-phase.

$\varkappa$-Phase. Finally we shall discuss possible charge orders in the $\varkappa$-phase. The Coulomb repulsions, V, are listed in Table 1. The results of the point charge approximation (Eq. 5) agree well with those of the direct integration (Eq. 4). These values are in good agreement with the reported results as well.[25,38] The largest V is the intradimer interaction (b1), 3.56 eV; this corresponds to the face-to-face limit (the right end) of Fig. 4, and the left end of V_c in Fig. 5. The second largest are the p interactions (2.9 eV), which can be estimated from Fig. 6. The q and b2 interactions are smaller than these interactions, and are nearly the same. Approximately these V values are inversely proportional to the intermolecular distances, R_0.

If the dimer of the $\varkappa$-phase is regarded as a unit, the $\varkappa$-phase has the same network of intermolecular interactions as θ-phase, where the b1 interaction in the $\varkappa$-phase corresponds to the c interaction in the θ-phase, and the p and q interactions are replaced by the p interaction (Fig. 14 in Ref. 7). The resulting hypothetical θ-phase is, however, effectively half-filled, because each dimer unit contains one positive charge.

Because the network of the intermolecular interactions is the same, the discussion which led to the phase diagram in the atomic limit (Fig. 7) is valid for the $\varkappa$-phase as well, although Fig. 12 cannot be applied for the half-filled system. From Table 1, V_p ($+V_q$) is obviously larger than V_{b2}; this results in $V_p > V_c$ in the corresponding θ-phase. As a consequence, the vertical stripe will be realized, if any charge disproportionation takes place in the $\varkappa$-phase. It should be remarked that this vertical stripe does not change the size of the unit cell, whereas the horizontal or diagonal stripe doubles the unit cell.

The charge separation has been actually observed in such $\varkappa$-phases as (BEDT-TTF)$_4$PtCl$_6$PhCN and (BEDT-TTF)$_4$(Et$_4$N)M(CN)$_6$(H$_2$O)$_3$ [M = Fe and Co].[39,40] Charge disproportionation in the former compound is evident from the usual structure analysis, where each dimer has 2+ or 0 charge. The latter compounds show structural phase transitions around 150 K, suggesting a similar charge disproportionation. Both of these compounds have non magnetic ground states, strongly indicating the charge separation, be-

Table 1. Intermolecular Overlap Integrals, S, Coulomb Repulsions, V, and Distances, R_0, in $\varkappa$-(BEDT-TTF)$_2$Cu(NCS)$_2$ at 104 K[7]

	$S/\times10^{-3}$	V(PC)[a]/eV	V(Int)[b]/eV	R_0/Å
b1	27.2	3.56	3.57	3.91
b2	11.1	2.49	2.47	6.54
p	11.9	2.89	2.89	5.36
p′	10.5	2.85	2.84	5.47
q	−1.8	2.50	2.48	6.49
q′	−3.1	2.45	2.43	6.68

a) Point charge approximation according to Eq. 5. b) Direct integration according to Eq. 4.

cause (completely) charge separated states in these effectively half-filled systems are inevitably non magnetic. It should be emphasized that charge order in the half-filled system takes place at the cost of spin polarization as well as the kinetic energy. This is the reason that the Mott insulator (or antiferromagnetic) phase is comparatively stable in the $\varkappa$-phase.

When we discuss the magnetic structure of the $\varkappa$-phase, we can use the phase diagram of Fig. 13. From Table 1, $|t_p|+|t_q|$ is larger than $|t_{b2}|$, resulting in $|J_p| > |J_c|$. Consequently, the vertical antiferromagnetic phase is expected as the magnetic order of the $\varkappa$-phase.

Conclusion

In the present work, various charge ordered states are understood by the combination of two phase diagrams. One is that of the atomic limit (Fig. 7 or more generally Fig. 9), where the charge order takes place in the direction of the smallest V. Another phase diagram is Fig. 12, which represents how V competes with U and W. The model presented here is a simplified two-dimensional version of the well studied quarter-filled uniform system.[30] It is expected that the charge order will be observed universally in organic conductors with nearly uniform (or weakly dimerized) structures.

References

1 K. Hiraki and K. Kanoda, *Phys. Rev.*, **B54**, 17276 (1996); K. Hiraki and K. Kanoda, *Phys. Rev. Lett.*, **80**, 4737 (1998).

2 T. Yamamoto, H. Tajima, J. Yamaura, S. Aonuma, and R. Kato, *J. Phys. Soc. Jpn.*, **68**, 1384 (1999).

3 J. Dong, K. Yakushi, K. Takimiya, and T. Otsubo, *J. Phys. Soc. Jpn.*, **67**, 971 (1998).

4 H. Mori, S. Tanaka, T. Mori, and Y. Maruyama, *Bull. Chem. Soc. Jpn.*, **68**, 1136 (1995).

5 H. Mori, S. Tanaka, and T. Mori, *Mol. Cryst. Liq. Cryst.*, **284**, 15 (1996).

6 H. Mori, S. Tanaka, and T. Mori, *Phys. Rev. B*, **57**, 12023 (1998).

7 T. Mori, H. Mori, and S. Tanaka, *Bull. Chem. Soc. Jpn.*, **72**, 179 (1999).

8 K. Hiraki, R. Chiba, T. Takahashi, and T. Nakamura, private communication.

9 K. Miyagawa, A. Kawamoto, and K. Kanoda, *Phys. Rev. Lett.*, in press.

10 H. Mori, S. Tanaka, T. Mori, A. Kobayashi, and H. Kobayashi, *Bull. Chem. Soc. Jpn.*, **71**, 797 (1998).

11 H. Tajima, S. Kyoden, H. Mori, and S. Tanaka, *Phys. Rev. B*, in press.

12 T. Mori, A. Kobayashi, Y. Sasaki, H. Kobayashi, G. Saito, and H. Inokuchi, *Bull. Chem. Soc. Jpn.*, **57**, 627 (1984).

13 J. Wosnitza, "Fermi Surfaces of Low-Dimensional Organic Metals and Superconductors," Springer, Berlin (1996).

14 T. Mori, *Bull. Chem. Soc. Jpn.*, **71**, 2509 (1998).

15 H. Kino and H. Fukuyama, *J. Phys. Soc. Jpn.*, **64**, 1877 (1995).

16 H. Kino and H. Fukuyama, *J. Phys. Soc. Jpn.*, **64**, 2726 (1995).

17 H. Kino and H. Fukuyama, *J. Phys. Soc. Jpn.*, **64**, 4523 (1995).

18 H. Kino and H. Fukuyama, *J. Phys. Soc. Jpn.*, **65**, 2158 (1996).

19 H. Seo and H. Fukuyama, *J. Phys. Soc. Jpn.*, **66**, 3352 (1997).

20 H. Seo and H. Fukuyama, *J. Phys. Soc. Jpn.*, **67**, 1848 (1998).

21 H. Seo, *J. Phys. Soc. Jpn.*, **69**, 805 (2000).

22 T. Mori, *Bull. Chem. Soc. Jpn.*, **72**, 2011 (1999).

23 H. Sato, E. Ishiguro, M. Kobori, and M. Asano, *Computer Center News (the University of Tokyo)*, **8** Suppl. 2, 21 (1973).

24 F. Castet, A. Fitsch, and L. Ducasse, *J. Phys. I France*, **6**, 583 (1996).

25 Y. Imamura, S. Ten-no, K. Yonemitsu, and Y. Tanimura, *J. Chem. Phys.*, **111**, 5986 (1999).

26 A similar factor is found in, K. Dichtel, R. J. Jelitto, and H. Koppe, *Z. Phys.*, **246**, 248 (1971); *Z. Phys.*, **251**, 173 (1972).

27 E. C. Stoner, *J. Phys. Radium*, **12**, 372 (1931).

28 D. R. Penn, *Phys. Rev.*, **142**, 350 (1966).

29 J. E. Hirsch, *Phys. Rev. B*, **31**, 4403 (1985).

30 J. E. Hirsch and D. J. Scalapino, *Phys. Rev. Lett.*, **50**, 1168 (1983); *Phys. Rev. B*, **27**, 7169 (1983).

31 R. Chiba, T. Nakamura, and T. Takahashi, in preparation.

32 T. Nakamura, R. Kinami, W. Minagawa, T. Takahashi, H. Mori, S. Tanaka, and T. Mori, *Synth. Metals*, **86**, 1991 (1997).

33 T. Nakamura, W. Minagawa, R. Kinami, and T. Takahashi, *J. Phys. Soc. Jpn.*, **69**, 504 (2000).

34 T. Nakamura, W. Minagawa, R. Kinami, Y. Konishi, and T. Takahashi, *Synth. Metals*, **103**, 1898 (1999).

35 D. Jerome, *Science*, **252**, 1509 (1991).

36 H. Kino and H. Kontani, *J. Phys. Soc. Jpn.*, **68**, 1481 (1999).

37 K. Kanoda, *Hyperfine Int.*, **104**, 235 (1997).

38 L. Ducasse, A. Frisch, and F. Castet, *Synth. Metals*, **85**, 1627 (1997).

39 A. A. Galimzyanov, A. A. Ignatèv, N. D. Kushch, V. N. Laukhin, M. K. Makova, V. A. Merzhanov, L. P. Rozenberg, R. P. Shivaeva, and E. B. Yagubskii, *Synth. Metals*, **33**, 81 (1989).

40 P. L. Magueres, L. Ouahab, N. Conan, C. J. Gomez-Garcia, P. Delhaes, J. Even, and M. Bertault, *Solid State Commun.*, **97**, 27 (1996).